Laboratory Report
of
National Metrology Institute of Japan (NMIJ/AIST)
and Japan Electric Meters Inspection Corporation (JEMIC)
2021-2023

At NMIJ/AIST, there are five research groups in the electrical standards area. They are the Applied Electrical Standards Group, the Quantum Electrical Standards Group, the Radio-Frequency Standards Group, the Electromagnetic Fields Standards Group, and the Electromagnetic Measurement Group.

The Applied Electrical Standards Group takes charge of the AC/DC transfer, the impedance and the power standards. The Quantum Electrical Standards Group covers the Josephson voltage and the quantum Hall resistance standards.

The Radio-Frequency Standards Group takes charge of RF power, voltage, noise, and attenuation standards. The Electromagnetic Fields Standards Group covers antenna properties, electric field and magnetic field standards. The Electromagnetic Measurement Group takes charge of RF impedance (S-parameter) standards and material properties.

This report also includes an overview of the digitalization projects undertaken at NMIJ and their specific implementation in the area of electrical standards as in the last section.

1. Josephson Voltage

1.1 PJVS operation in dilution refregirator system

A liquid-helium-free PJVS cooled with a GM cooler has been utilized since 2015 for calibrations of Zener voltage standards with the CMC values, 8 nV for 1 V and 45 nV for 10 V, same as those for our conventional JVS system cooled with liquid helium. We are now attempting to operate the PJVS chip on the 4 K stage in a dilution refrigerator system toward the quantum-metrology-triangle measurement and other general applications. Up to now, we have succeeded in the stable temperature control of the sample stages and the stable generation of the quantized voltage steps. (Contact: Daiki Matsumaru, d-matsumaru@aist.go.jp).

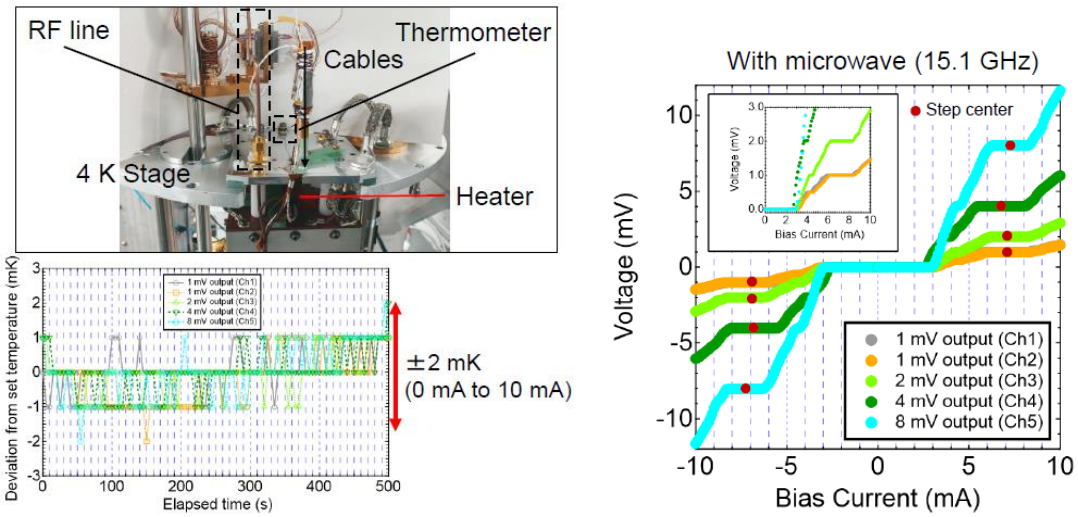

Fig.1 Implementation of PJVS module in a dilution refriqerator, temperature stability of 10 K stage, and quantized voltage steps generated from the PJVS.

1.2 Thermodynamic temperature measurement

We measured the thermodynamic temperature of the melting point of gallium T_{Ga} using a Johnson noise thermometer (JNT) with an integrated quantum voltage noise source (IQVNS) as a reference. T_{Ga} was calculated using the fundamental constants recommended by the Committee on Data for Science and Technology (CODATA) for the revision of the International System of Units (SI). The measured T_{Ga} is consistent with the value defined in the International Temperature Scale of 1990.The power spectral density of output signal of IQVNS has been fixed so far. In order to use IQVNS as a reference for the measurement of thermodynamic temperature at various temperature fixed points, the power spectral density of the output signal of IQVNS should be variable. We improved part of the design of the device to be able to change the power spectral density of the output signal. (Contact: Chiharu Urano, c-urano@aist.go.jp).

2. Resistance

2.1 Standard Resistors

Development of compact and ultra-stable 1 Ω and 1 kΩ standard resistors has been finished, and resistors with 10 kΩ are in progress of evaluation and development. The best resistors display extremely small average drift rates and temperature coefficients, and other performances, e.g.,

- 1 Ω: 4.2 nΩ/(Ω year), 4 nΩ/(Ω ˚C) at 23 ˚C,
- 10 Ω: 0.53 nΩ/(Ω year), 1 nΩ/(Ω ˚C) at 23 ˚C,
- 100 Ω: 50 nΩ/(Ω year), < 20 nΩ/(Ω ˚C) at 23 ˚C, deviation by transportation:

< 10 nΩ/Ω, power and humidity coefficients are negligible,

- 1 kΩ: < 10 nΩ/(Ω year), 1.7 nΩ/(Ω ˚C) at 23 ◦C.

(note that the average drift rate and temperature coefficient of each resistance value does not come from the same resistor). It is demonstrated that this excellent performance is suitable for utilization in national metrology institutes and international comparisons.

Development of stable high-resistance standard resistors is also undergoing, and the developed resistors are now commercially available as type HVR10000 series from Japan Finechem corporation. The development is done mainly in 100 GΩ and the developed resistors show a small temperature coefficient of less than 5 (μΩ/Ω)/K and the other characteristics are also good.

(Contact: Takehiko Oe, t.oe@aist.go.jp).

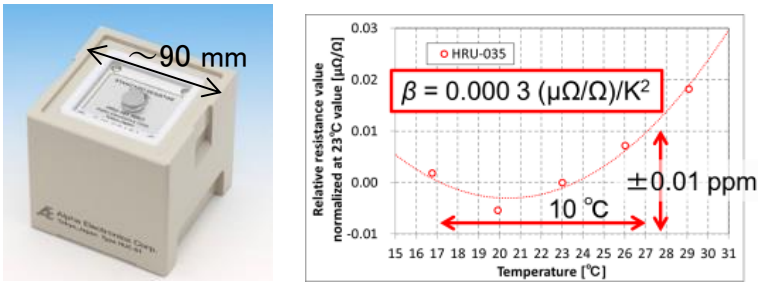

Fig. 2 Picture and temperature-resistance curve of developed 100 Ω standard resistor.

Fig. 3 Developed high-resistance standard resistor, HVR10000 series made by Japan Finechem corporation.

2.2 DC high-resistance comparison between NIST and NMIJ

A precise high resistance comparison was performed between the traveling dual source bridge developed by the National Metrology Institute of Japan (NMIJ) and the adapted Wheatstone bridge of the National Institute of Standards and Technology (NIST) from 10 MΩ to 100 TΩ at NIST. The NMIJ traveling bridge was shipped to NIST Gaithersburg and was installed right next to the NIST bridge and these bridges alternately measured the resistance ratio of the high resistance standards, without moving the location of the resistors inside the temperature controlled air-bath. Having the bridges and resistance standards in the same location for the comparison decreased the transportation and

temperature coefficient effects on the resistance standards, contributing to the excellent agreement of the measured values. The NMIJ traveling bridge used an 8.5-digit digital multimeter and a relay switch box to determine a resistance ratio by measuring the ratio of the voltages applied to the resistors. The comparison was started from 10 MΩ based on the same 1 MΩ standard resistor calibrated using a NIST two-terminal cryogenic current comparator bridge, and standard resistors from 10 MΩ to 100 TΩ were calibrated by repeating 10 : 1 scaling measurements with both systems. Excellent agreement was obtained within the uncertainty of all resistance ranges and the difference between both systems was less than 1 μΩ/Ω up to 1 TΩ and the degrees of equivalence for 10 TΩ and 100 TΩ were less than 6 μΩ/Ω [1] (Contact: Takehiko Oe, t.oe@aist.go.jp).

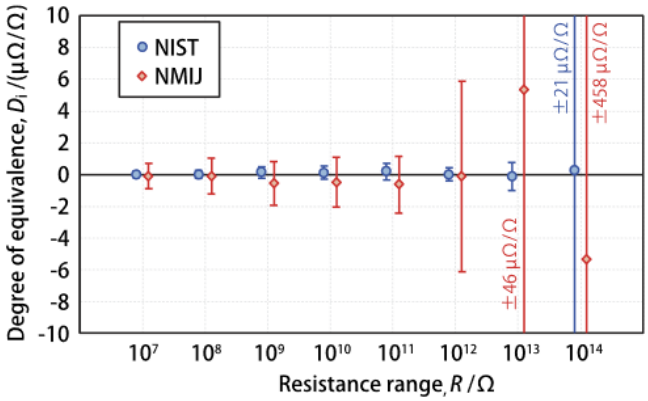

Fig. 4 .DoE for the measurements from 10 MΩ to 100 TΩ between NIST and NMIJ [1].

2.3 Contact Resistance Evaluation of Wire Harness

To establish a relationship between the physical structure of electrical contact boundary and contact resistance, NMIJ developed a method for evaluating that using a physical simulated sample created via nanofabrication. Several samples with various distribution of "contact area" were made and their resistances were measured precisely. It was demonstrated experimentally that our result is in good agreement with an expression for constriction resistance.

Impedance measurement was introduced as a degradation diagnosis method for contacts of wire harness by a nondestructive test. It was found that the changes in reactance at a certain frequency behave characteristically and independently of the DC resistance changes during accelerated test. The degradation degree of contacts was estimated by the change in impedance. (Contact: Yasuhiro Fukuyama, y.fukuyama@aist.go.jp).

3. DC Current (single electron pumping)

Towards a realization of the current standard based on the single-electron pumping, we investigate the physics of low-temperature electron transport phenomena in various types of single-electron devices, i.e. superconductor-insulator-normal- insulator-superconductor (SINIS) turnstiles, gate-confined quantum dots, and graphene- or nanotube-based single-electron transistors.

On SINIS turnstiles, in our early studies, we had discovered the new phenomenon that is a reduction of the single-electron pumping error induced by a weak magnetic field applied to the device. The origin of this phenomenon is related to the suppression of inverse-proximity effect at the interface between superconducting leads and a normal metal island. The inverse proximity effect cause the quasiparticle trap at the interface, namely it leads to the overheating of the junction. The magnetic field weaken the inverse proximity effect and helps to lease the quasiparticle. We justify this scenario from numerical analysis and controlling the tunnel resistance. Aiming at further reducing the pumping error, we extended the research to that based on another pumping mechanism. In one instance, we investigated a GaAs-based gate-defined quantum dot and demonstrated single-parameter pumping. In addition, we developed an air-bridge based parallel integration of this pump to demonstrate a synchronized parallel pumping that can generate a larger current otherwise unattained. In this study, we succeded to operate the GaAs single electron device with sigma-delata madulated pulses for the arbitrary wave generation. This technique is thought to be useful for the calibration of current noise in the shot noise measurement. Also we start to measure the Si single electron pump device in collaboration with NTT group. At present we succeded to operate single electron pumping at 1 GHz with 10^{-6} uncertainty. Also we are trying to operate this type of device in parallel to generate large (a few nano ampere) current. Four silicon pump devices are simulateously operated at 1 GHz with 10^{-6} uncertainty levels inside dilution refrigerator. To test the uncertainty of pumped current, we are trying to compare the generated current each others.

These single-electron devices are planned to be integrated with the quantum metrology triangle experiment that combine the single-electron device with the quantum Hall resistance and Josephson voltage standards. Towards this futuristic experiment, we had introduced a dry dilution refrigerator; An ample open space offered by this refrigerator allows us to integrate the whole components required for the triangle experiment including a cryogenic current comparator into one system. Electric noise filters and high-frequency wiring are now designed and constructed to complete this setup. Also to operate Josephson voltage standard and quantum Hall array device inside the dilution refrigerator, we are installing additional cold stage and try to operate these quantum standards. As a

result, we succeeded to operate Josephoson voltage standard inside a dilution refregerator. We obtained 1 V with 4.8 $\times 10^{-10}$ and 2 mV with 4.3×10^{-8}. (Contact: Shuji Nakamura, shuji.nakamura@aist.go.jp).

4. LF-Impedance

AC resistor calibration service has been kept in the range of 10 kΩ at 1 kHz. Standard capacitor (dry-nitrogen or used silica dielectric) calibration service has been kept in the range of 10 pF up to 1000 pF at 1.592 kHz. (Contact: Atsushi Domae, domae-atsushi@aist.go.jp).

NMIJ has started a development of precision measuring techniques for diagnosis of the energy storage devices such as lithium-ion batteries and super-capacitors by using an impedance spectroscopy method. We have a plan to establish a metrology for evaluating the storage power devices. Preliminary impedance measurements for lithium-ion battery cells in the range of 10 mHz – 10 kHz demonstrated that the impedance value for unused cells is clearly distinguished from that for used-up cells. Impedance spectra for the unused cells which are obtained under 100 mΩ indicate that the evaluations of the uncertainties should be required for detecting a faint sign or a symptom of degradations of storage devices. We have developed an electrochemical impedance measurement system and have evaluated the type-A uncertainty for the impedance spectra which was estimated to be less than 0.2 mΩ.

AIST established the Global Zero Emission Research Center (GZR) in 2020. GZR has a mission for an international joint research base for zero emission technologies. GZR started to research for innovative environmental and energy technologies, including in the fields of renewable energy, storage batteries, hydrogen, and so on. NMIJ joined in GZR and has started the research of the safety and reliability evaluation method for solid oxide electrochemical cells and lithium ion batteries by using precision impedance and charge-discharge measurements.

(Contact: Norihiko Sakamoto, n-sakamoto@aist.go.jp).

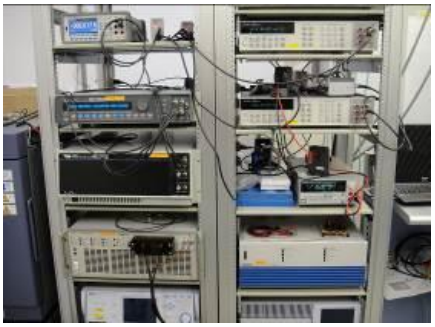

Fig. 5 Photograph of the electrochemical impedance measurement system developed using the Frequency Response Analyzer and the Potentio-Galvano Stat.

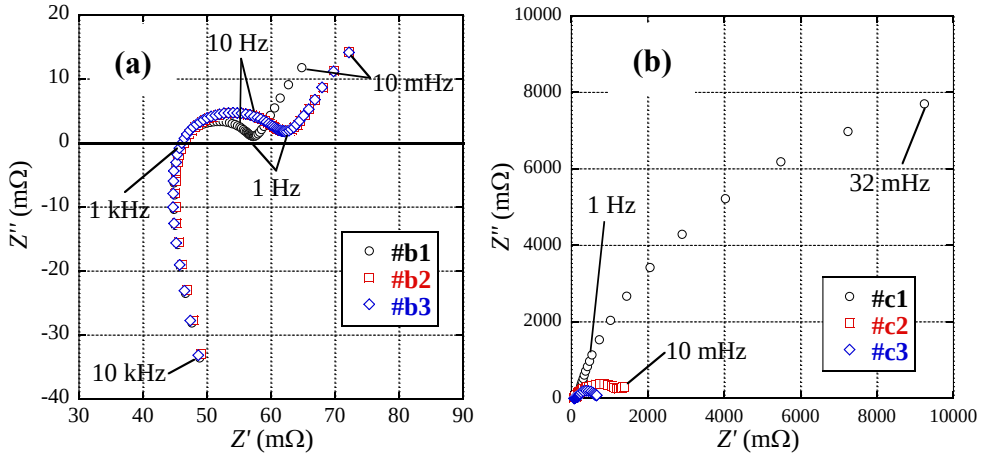

Fig. 6 Nyquist plot of the impedance spectra for the 18650-type lithium-ion batteries: (a) the unused samples and (b) used-up samples. Obvious change in impedance spectra was observed with the progression of the charge/discharge cycle.

5. AC/DC transfer

NMIJ has provided ac-dc voltage difference transfer calibration of thermal converters in the voltage range from 10 mV to 1000 V and in the frequency range from 10 Hz to 1 MHz, and AC voltage calibration below 10 Hz. We have been participating in APMP. EM-K12 comparison[2], and CCEM-K6a/K9 key comparison[3].

The thin film multi-junction thermal converters with a novel design have been developed in collaboration with NIKKOHM co. ltd. We have introduced a new thermopile pattern to improve the performance of our thin film MJTC[4]. Using these thermal convertes, novel thermal converter circuits arranged in an 2 by 2 matrix have been fabricated to improve the low-frequency AC-DC transfer differences[5]. Thin-film AC-DC resistor on an aluminum nitride (AlN) substrate with negligible voltage dependence have been fabricated for measuring AC voltages up to 1000 V[6]. Toward next-generation AC/DC current transfer standard, high-current multijunction thermal conveters on a Si substrate up to 1 A have been designed and fabricated through the collaborative project with National Institute of Standards and Technology in Gaithersburg[7].

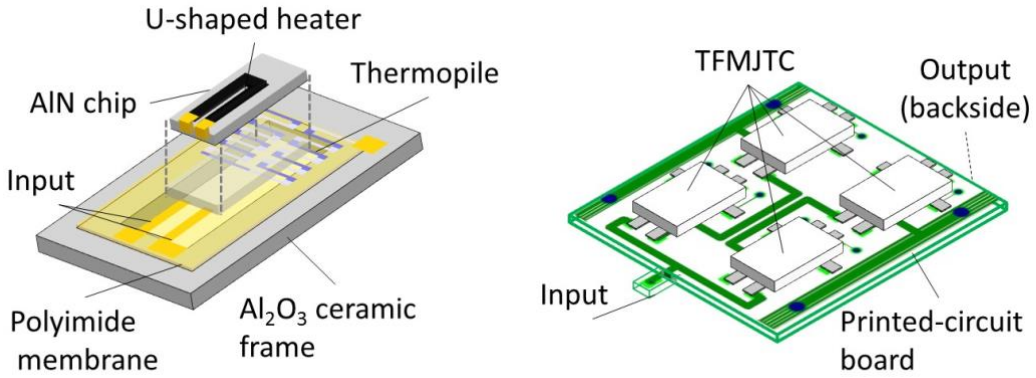

Fig. 7

Toward quantum AC voltage standards, a differential sampling measurement system using an AC-programmable Josephson voltage standard (AC-PJVS) system has been developed[8]. To extend the voltage range of the system, we have combined an two-stage inductive voltage divider and an 10 V AC-programmable Josephson voltage standard chip.

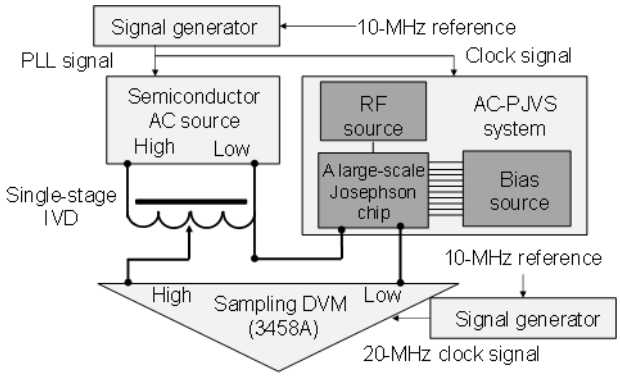

Fig. 8

Toward a waste-heat recovery with thermoelectric conversion, we have developed advanced metrology techniques and apparatus using a precise ac and dc electrical measurement technique. The Seebeck coefficient is an essential indicator of the conversion efficiency and the most widely measured property specific to these materials. So far, we have developed a method to precisely measure Thomson effect to determine the absolute Seebeck coefficient of platinum reference material[9,10]. (Contact: Yasutaka Amagai, y-amagai@aist.go.jp, Kenjiro Okawa, okawa.k@aist.go.jp).

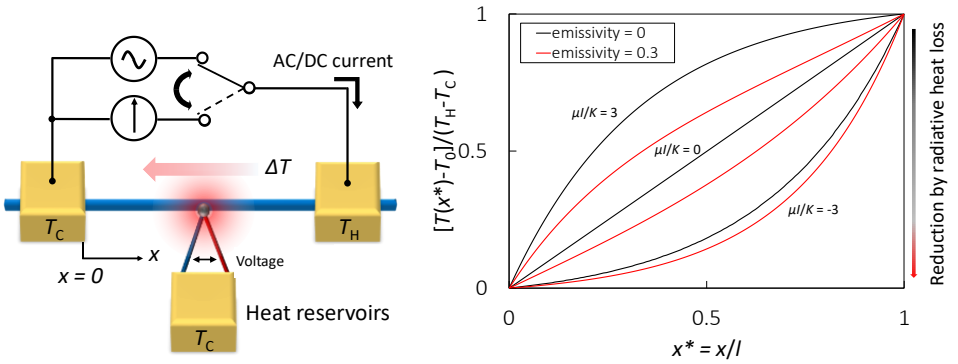

Fig. 9

6. Power (NMIJ)

6.1. Power at NMIJ (harmonics, etc)

An improved evaluation system for a wideband resistive voltage divider (WRVD) is under development. The fabrication of an accurate and precise WRVD based on the extended Hamon method has been realized by direct soldering of series resistor and by soldering on the edge of round substrates for parallel resistor with suitable fixtures. The improved evaluation system was verified with calibrated IVDs. By replacing with a phase standard, the difference from the calibration result by Thompson's method has been effectively reduced comparing with the previous system. An error simulation of the equivalent circuit of the IVDs based on the calibration result has revealed the large quadrature error of the improved system at 50 kHz. It was considered due to the phase error of the phase standard. (Contact: Tatsuji Yamada, yamada.79@aist.go.jp)

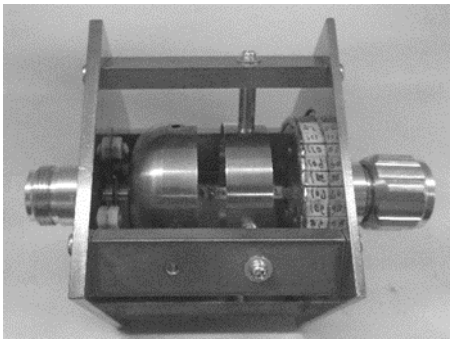

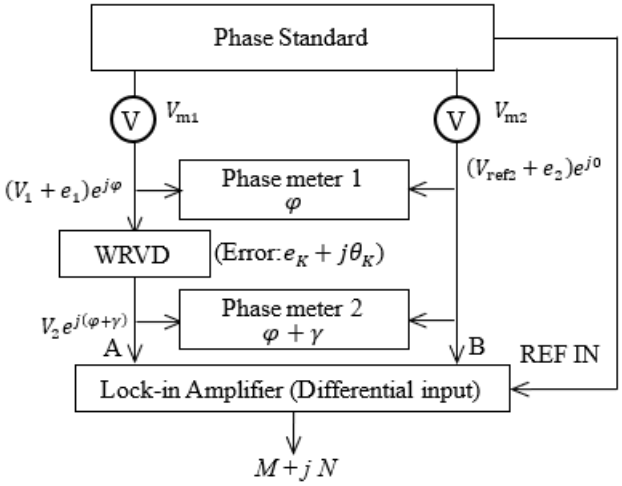

Fig. 10

6.2. Power at JEMIC (mains)

JEMIC has provided the primary active/reactive power/energy standards for the power

frequencies in the voltage range from 50 V to 120 V and in the current range from 2.5 A to 50 A. The standard individually measures voltage U and current I with two precise voltmeters and a shunt resistor, and phase θ with a precise digital phase meter. After these measurements, the active and reactive powers are calculated by UIcosθ and UIsinθ, respectively. The representative expanded uncertainties under conditions of 100 V and 5 A are 22 μW/VA (power factor 1) and 10 μW/VA (power factor 0). In 2021, we calibrated approximately 10 power meters and 20 energy meters.

JEMIC has been participating in APMP Key Comparison for APMP.EM-K5.1 of AC power and energy[12]. (Contact: TADOKORO Takuya, t-tadokoro@jemic.go.jp)

7. RF-Power

NMIJ developed a WR-5 waveguide-based calorimeter for the frequency range of 140-220 GHz in collaboration with the National Institute of Information and Communication Technology. Direct comparison calibration was demonstrated for commercially available power meters using the calorimetr as a reference standard. We have begun to provide reference values for the WR-5 band to domestic organizations.

(Contact: Yuya Tojima, yuya-tojima@aist.go.jp, Moto Kinoshita, moto-kinoshita @aist.go.jp)

8. RF-Attenuation and Phase Shift

NMIJ has established national standard for RF and microwave attenuation in the frequency range of 1 kHz to 110 GHz, and provides its calibration services mainly with the Japan Calibration Service System (JCSS) scheme. All measurement and calibration systems work based on the intermediate frequency (IF) substitution method using the highly accurate null detection and employing an inductive voltage divider (IVD) as the reference standard. A recent improvement was the inclusion of a new measurement system in the frequency range of 1 kHz to 100 kHz, as shown in Fig. 11 to meet industry requirements for electromagnetic compatibility (EMC) [13] .

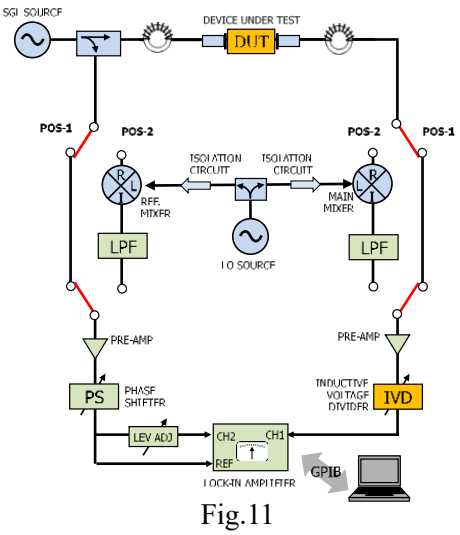

Fig.11

These systems have been commercially manufactured by 7Gaa Corporation (https://7gaa.co.jp/) and several have been shipped to overseas NMIs for use as their national RF attenuation standards.

NMIJ established national standard for RF phase shift in the frequency range of 10 MHz to 1 GHz. The expanded uncertainties are 0.029° for DUT with losses up to 20 dB, 0.031° for 40 dB, and 0.056° for 60 dB loss. The frequency range is currently being expanded to 18 GHz [13][14].

NMIJ took an initiative to organize a CIPM Key Comparison of attenuation at 18 GHz, 26.5 GHz and 40 GHz using a step attenuator (CCEM.RF-K26) [16]. Measurements of both the first and second round loop were completed on February 2018. It can be said successful, although there were some delays in the delivery of the traveling standards between the participants. The Draft B Report is currently under review by the CCEM members.
(Contact: Anton Widarta, anton-widarta@aist.go.jp, Moto Kinoshita, moto-kinoshita@aist.go.jp)

9. RF-Impedance and related measurement technology

NMIJ researched the precision on-wafer measurement techniques over 100 GHz and developed a full-automatic RF probing system establishing high reproducibility of measurements. Balanced type circular disk resonator method has been developped and commarcialized, in addition, the method will be published as an IEC standardization. The method cannot only measure dielectric permittivity but also conductivity at millimeter wave frequency (Fig.12). Furthermore, electromagnetic sensing techniques is also researching for the agriculture products, food and infrastrucre, etc.

NMIJ as a pilot laboratory is managing the CCEM key comparison (CCEM.RF-K5c.CL: S-parameter for PC3.5 in the range from 50 MHz to 33 GHz) [17], the APMP supplemental comparison (APMP.EM.RF-S5.CL: Dimensionally-derived characteristic impedance for PC7, PC2.4 and PC1.85) [18] and the pilot study for material characterization.

Calibration certificates for S-parameter measurements using the vector network analyzers have been digitized. Six calibration certificates were issued in November 2022.
(Contact: Ryoko Kishikawa, ryoko-kishikawa@aist.go.jp, Yuto Kato, y-katou@aist.go.jp, Seitaro Kon, seitaro-kon@aist.go.jp)

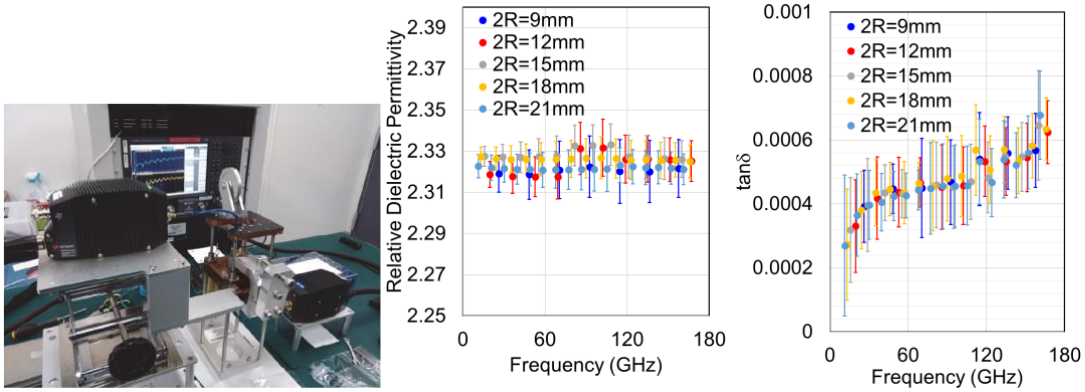

Fig. 12 Balanced type circular disk resonator at millimeterwave frequency

10. Antennas, electric field, and magnetic field

A calibration service for the free-space antenna factor on loop antenna is maintained in the frequency range of 20 Hz to 30 MHz. The expanded uncertainty of the magnetic antenna factor was improved to be from 0.4 dB to 0.7 dB in the frequency range from 9 kHz to 30 MHz in December 2019 [19,20].

AC Magnetic field sensor calibration service is maintained in a range of 1 uT to 150 uT from 50 Hz to 100 kHz [21]. The realizable field strength depends on frequency points.

NMIJ is also developing a novel EM-sensor and a EM visualization method by using quantum phenomena of vapor cesium atoms [22-25].
(Contact: Masanori Ishii, masanori-ishii@aist.go.jp)

Calibration of the dipole antenna factor above a ground plane from 30 MHz to 1 GHz with the specific conditions (with horizontal polarization and at 2.0 m from the ground plane surface) is available. Since EMC (electromagnetic compatibility) measurements are ordinarily carried out in free space above 1 GHz, the dipole antenna factor from 1 GHz to 2 GHz is calibrated in an anechoic chamber. The free space dipole factor is one of the traceability source of the E-field strength calibration in free space [26], [27].
(Contact: Takehiro Morioka, t-morioka@aist.go.jp)

The free space antenna factor calibration services for broadband antenna for Biconical antenna (30 MHz to 300 MHz), Log periodic dipole array antenna (300 MHz to 1000 MHz) and Super broadband antenna (30 MHz to 1000 MHz) are being performed using our original three antenna calibration method [28-30]. The ten calibration services

have been provided to the client in between 2019 and 2021. In 2022, we digitized calibration certificates for broadband antennas and provided the client with four digitized calibration certificates.
(Contact: Sayaka Matsukawa, sayaka-matsukawa@aist.go.jp)

Calibration services for the gains of standard horn antennas are being performed from 18 GHz to 40 GHz using the extrapolation method. An antenna factor calibration service for the broadband horn antenna (1 GHz to 18 GHz) is available using the time-domain single antenna extrapolation method in the semi-anechoic chamber.
(Contact: Yuanfeng She, yuanfeng.she@aist.go.jp)

An antenna gain calibration service for millimeter-wave standard gain horn antenna are being performed form 50 GHz to 75 GHz and 75 GHz to 110 GHz using a time-domain processing and extrapolation technique. Standard gain horn antenna calibration service for 220 GHz to 330 GHz has been started from March 2020. The expanded uncertainty of antenna gain was estimated to between 0.34 dB to 0.5 dB. The mm-wave antenna gain calibration by single antenna extrapolation method with moving flat-reflector is also studied [31-34].

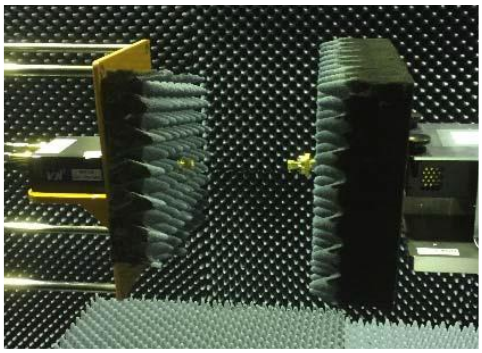

Fig. 13 Antenna gain calibration system for 220 to 330 GHz

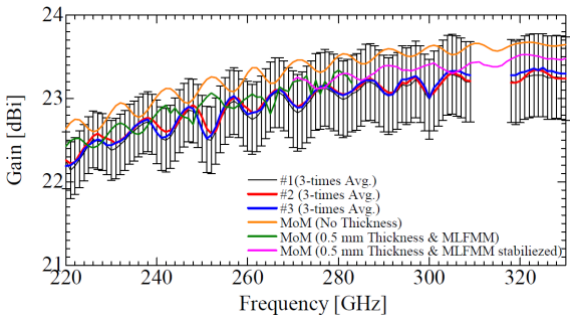

Fig. 14 Estimated antenna gain that compare with MoM results

Radar Cross Section (RCS) calibration service for cylindrical metal reflector and square metal plate in W-band has been started from March 2019 (Fig. 15). The expanded uncertainty of RCS for cylindrical metal reflector in W-band was estimated to between 1.1 to 1.6 dB. The expanded uncertainty of RCS for square metal plate reflector in W-band was estimated to between 1.4 dB to 2.1 dB.

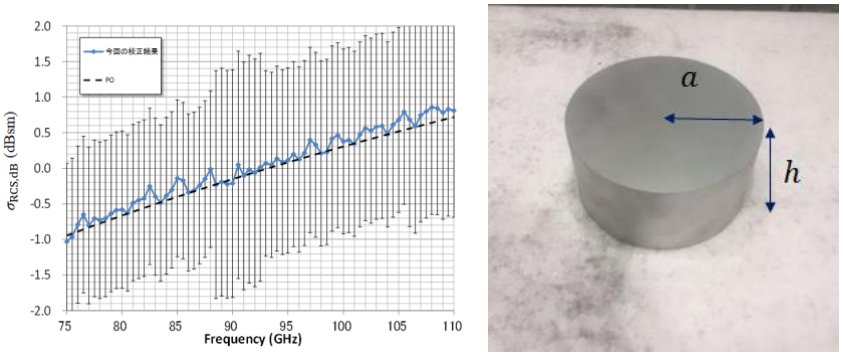

Fig. 15 RCS calibration results in W-band and an example of a cylindrical reflector
(Contact: Michitaka Ameya, m.ameya@aist.go.jp)

The E-field strength is one of the important quantities in the electromagnetic free field metrology and the field measurement is ordinarily carried out by using a calibrated E-field probe. In NMIJ/AIST, the correction factors of the E-field probe are calibrated against the field level of 10 V/m and 20 V/m generated in a G-TEM cell. Three appropriate methods to generate the standard E-field depending on the measurement frequency are employed in calibrating the response of the primary optical field transfer probe. A TEM cell is employed as a standard E-field generator at lower frequencies below 900 MHz, and the E-field level from 0.8 GHz to 2.2 GHz is calibrated by using the free space dipole antenna factor in the anechoic chamber. Antenna gain and the net power flowing into the transmitting antenna are the traceability souces for the standard field generation in the anechoic chamber from 2 GHz to 6 GHz. The optical E-field transfer probe calibrated against these standard E-fields transfers the E-field level into the G-TEM cell, and then the ordinary field probe is calibrated up to 4 GHz [35].
(Contact: Takehiro Morioka, t-morioka@aist.go.jp, Michitaka Ameya, m-ameya@aist.go.jp)

11. Terahertz Metrology

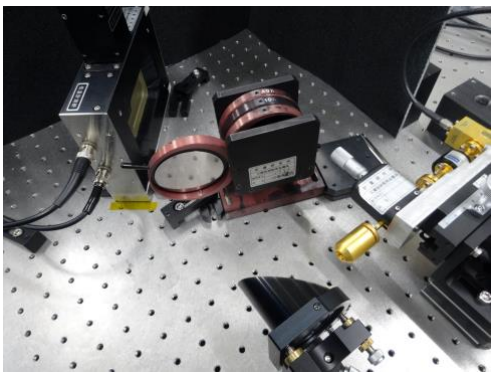

Fig. 16 Photograph of the THz attenuation calibration system for free-space beams.

NMIJ developed a method for measuring terahertz (THz) attenuation for free-space beams (Fig. 16). It employs a photo-acoustic detector to compare THz attenuation to audio-frequency (AF) attenuation. The AF attenuation is directly calibrated by an inductive voltage divider as a reference standard. Using a metalized-film attenuator, we have demonstrated attenuation measurements up to 20 dB for 0.11 THz collimated beams.
(Contact: Hitoshi Iida, h-iida@aist.go.jp, Moto Kinoshita, moto-kinoshita@aist.go.jp)

12. Material Characterization

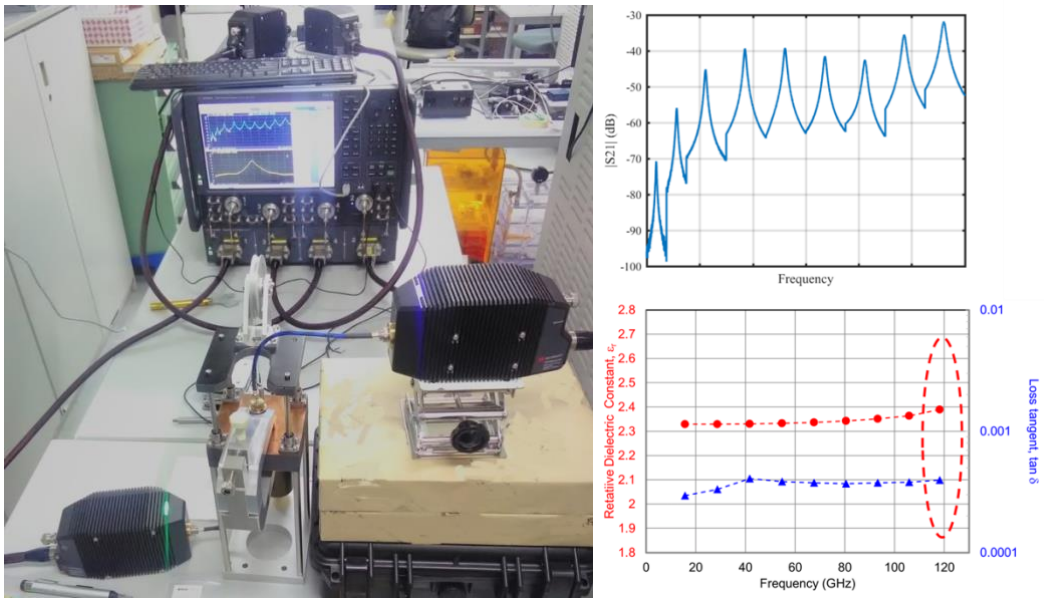

Fig. 17 Photographs of Balanced-type circular-disk resonator(BCDR) and Measurement Results of cyclic olefin polymers (COP) up to 120 GHz

NMIJ is researching and develops material characterization, i.e. dielectric permittivity measurements, at the millimeterwave frequency. NMIJ developed the Balanced-type circular-disk resonator(BCDR) and analytical sofware for dielectroic permittivity of low loss materials. Measurement can be perfformed in broad band frequency and up to 120 GHz (Fig. 17). The method is now being standardized in the IEC standard, then the system has been provided by the measurement instrument company.
Furthermore, NMIJ as a pilot laboratory manages the Pilot study for dielectric permittivity measurement proposed by NIST as a former pilot laboratory in it.
(Contact: Yuto Kato, y-katou@aist.go.jp, Seitaro Kon, seitaro-kon@aist.go.jp))

13. Digitalization

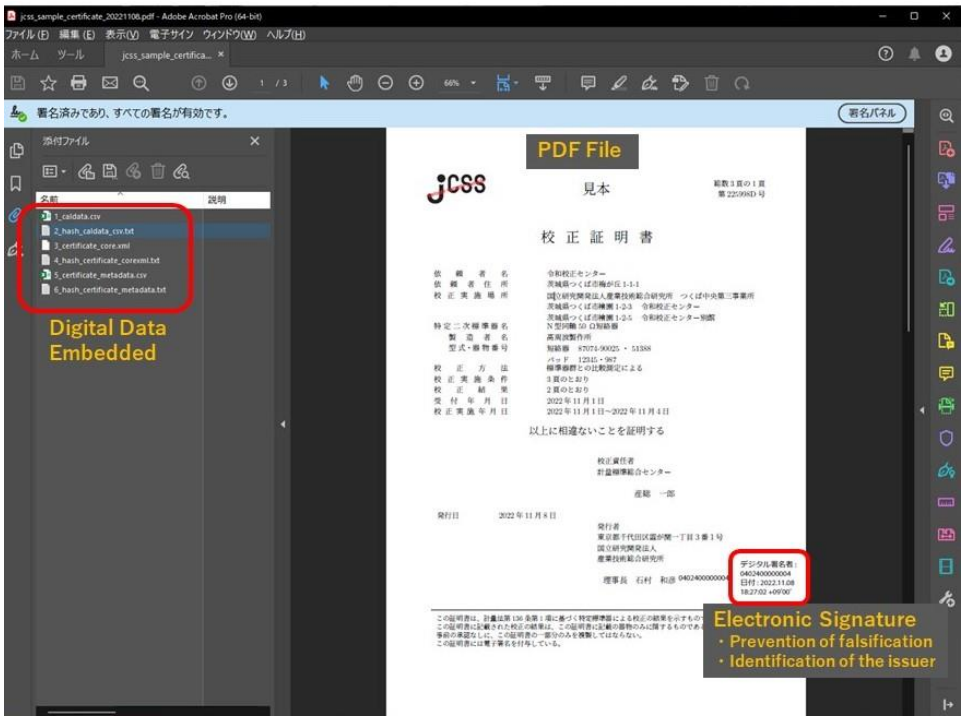

Fig. 18 A sample of NMIJ's DCC. The DCC is based on PDF with digital data embedded and secured by an electronic signagture.

NMIJ has initiated an official service for issuing Digital Calibration Certificates (DCC) from November 1, 2022. During the year 2022, NMIJ has carefully made interactions with domestic stakeholders upon their demands. Through such communication, we have identified that many of our stakeholders prefer to experience a moderate transition to digitalization. Having the leading examples such as the PTB's XML approach and the PDF approach proposed by METAS and some further investigations upon the ISO Standards related to PDF, we have selected the PDF approach to implement our first DCC to be issued under our governing domestic law. The PDF file has an appearance very similar to our existing calibration certificates issued on paper, however for the benefit of the customer, it also includes digital data embedded, such as the metadata of the calibration as well as calibration results in CSV format (Fig.18). Even such format will be a great benefit compared to paper certificates that contain a huge amount of data. Among approximately 600 service items that we provide, we still have only a few service items capable and ready for issuing DCCs. The number of DCCs issued has just exceeded 10, mostly from the electrical standards area with high data volumes, namely 6 DCCs for S-parameter measurements and 4 DCCs for broadband antenna measurements as mentioned in Sections 9 and 10, respectively. We have just stepped on the starting line

and will continuously improve our DCC format to fit the customer's demands. In addition, NMIJ actively promotes the benefits of using this DCC, including being a speaker or panelist at APMP-DXFG Webinar (Nov. 2022) [36] and 3rd International Digital Calibration Certificate (DCC) Conference (Feb. 2023) [37].

References

1. T. Oe, S. Payagala, A. R. Panna, S. Takada, N.-H. Kaneko, and D. G. Jarrett, "Precise high resistance comparison between the NMIJ traveling dual source bridge and the NIST adapted Wheatstone bridge", *Metrologia*, Vol. 59, No. 6, 065007, Oct. 2022.
2. APMP. EM-K12, Key comparison of AC-DC current transfer standards. (https://www1.bipm.org/kcdb/comparison?id=509)
3. CCEM-K6.a/K9, CIPM Key Comparison of AC-DC Voltage Transfer Standards.
4. H. Fujiki, Y. Amagai, K. Shimizume, K. Kishino, S. Hidaka, "Fabrication of Thin Film Multijunction Thermal Converters With Improved Long-Term Stability," *IEEE. Trans. Instrum. Meas*. Vol.64, No.6, Jan. 2015.
5. Y. Amagai, H. Fujiki, K. Okawa, N.-H. Kaneko, "Low-Frequency AC–DC Differences of a Series–Parallel Circuit of Thermal Converters," *IEEE. Trans. Instrum. Meas*. Vol.68, No.6. 2019.
6. H.Fujiki, Y. Amagai, and K. Okawa, "Establishment of High-Voltage AC–DC Voltage Transfer Standards in 1–100-kHz Range at NMIJ," *IEEE. Trans. Instrum. Meas*. Vol.68, No.6. 2019.
7. Y. Amagai, S. Cular. J. A. Hagmann, T. E. Lipe, N.-H. Kaneko "Low-Frequency Characteristics of Silicon-Based High-Current Multijunction Thermal Current Converters Fabricated by Wet Chemical Etching" *IEEE. Trans. Instrum. Meas*. Vol.70, 2021.
8. Y. Amagai, M. Maruyama, H. Yamamori, T. Shimazaki, K. Okawa, H. Fujiki, and N.-H. Kaneko, "Extending voltage range to 10 V rms in AC–DC difference measurements with AC programmable Josephson voltage standard" *Meas. Sci. Technol*. 31, 065010, 2020.
9. Y. Amagai, T. Shimazaki, K. Okawa, T. Kawae, H. Fujiki, and N.-H. Kaneko, "High-accuracy compensation of radiative heat loss in Thomson coefficient measurement," *Appl. Phys. Lett.* Vol. 117, 063903, August 2020.
10. Y. Amagai, T. Shimazaki, K. Okawa, T. Kawae, H. Fujiki, and N.-H. Kaneko, "Precise absolute Seebeck coefficient measurement and uncertainty analysis using high- T_c superconductors as a reference," *Rev. Sci. Instrum.* Vol.91, 14903, Jan. 2020.
11. T. Yamada and Y. Amagai, "Multiusing a TVC Toward Development of TVM-Based

Phase Measurement System up to 1 MHz," *IEEE. Trans. Instrum. Meas.* Vol. 70, 1503006, 2021.

12. https://www.bipm.org/kcdb/comparison?id=198
13. A. Widarta, "Primary standard of attenuation in the frequency range of 1 kHz to 10 MHz," in *CPEM Dig*., Denver, Co, Aug. 2020, *virtual*.
14. A. Widarta, "Precision phase shift measurement system in the frequency range of 1-18 GHz, *50th European Microwave Conf*., Utrecht, The Netherlands, Jan. 2021, *virtual*.
15. A. Widarta, "Working Standard for RF Attenuation and Phase-shift Calibrations," in *CPEM Dig*., Wellington, NZ, Dec. 2022.
16. https://www.bipm.org/kcdb/comparison?id=1016
17. https://www.bipm.org/kcdb/comparison?id=599
18. https://www.bipm.org/kcdb/comparison?id=333
19. M. Ishii, J. H. Kim, Y. Ji, and C. H. Cho, "Final report on APMP.RF-S21.F," *Metrologia* 55(1A):01003, January 2018.
20. https://www.bipm.org/kcdb/comparison?id=245
21. M. Ishii and M. Suzuki, "Impedance of Helmholtz Coils to Generate Standard AC Magnetic Fields in High Frequency," *2020 Conference on Precision Electromagnetic Measurements (CPEM)*, Aug. 2020.
22. M. Ishii and M. Kinoshita, "A feasibility study of a real-time visualization method for electromagnetic fields," *Microwave and Optical Technology Letters*, pp. 399-403, September 2020.
23. M. Ishii, "A study of frequency extension of AC magnetic field sensor using radio-optical multiple resonance in 133Cs," *EMC europe 2020*, Sep. 2020.
24. M. Kinoshita and M. Ishii, "Visualization of radio-frequency waves via double resonance spectroscopy of cesium atoms," *Japanese Journal of Applied Physics*, Vol. 58, No. 5, pp. 052004-1-5, April 2019.
25. M. Ishii, "A feasibity study of AC magnetic field sensor in low-frequency using multi radiooptical resonance in 133Cs," vol. 1, pp. 760, *Proceedings of EMC Sapporo & APEMC 2019*, June 2019.
26. T. Morioka, "Time-domain mixed-mode site attenuation measurement," *IEEE Trans. on Electromagn. Compat*., vol. 62, no. 6, pp. 2650-2660, Dec. 2020.
27. T. Morioka, "Improvement of anechoic chamber performance by the time-domain analysis," in *Proc. of EMC Sapporo and APEMC 2019*, Sapporo, Japan, June 2019
28. S. Matsukawa and S. Kurokawa, "Antenna gain self-calibration for Double Ridged Guide Horn Antenna using bi-directional optical fiber link transceiver", *ECTI-*

CON2019, pp. 1-4, Pattaya,Thailand, 10-13 July 2019.

29. S. Matsukawa, S. Kurokawa and, M. Hirose, “Uncertainty Analysis of Far-Field Gain Measurement of DRGH Using the Single-Antenna Method and Amplitude Center Distance”, *IEEE Tran. on Instrumentation and Measurement*, Vol. 68, No. 6, pp. 1756-1754, June 2019.
30. S. Matsukawa, S. Kurokawa, M. Ameya and Y. She, “Influence of reflection area on calibration accuracy by single antenna method using broadband antenna”, *CPEM2018*, pp. 1-2, Paris, France, 8-13 July, 2018.
31. M. Ameya, S. Matsukawa and S. Kurokawa, "Antenna Gain Self-calibration Method with Moving Flat Reflector for Millimeter-wave Frequency Band," *Proceedings of 2018 IEEE Conference on Antenna Measurements & Applications (CAMA)*, 2018
32. M. Ameya and S. Kurokawa, "Development of Antenna Gain Calibration System in 300 GHz Frequency Band", *Proceedings of 2019 URSI-Japan Radio Science Meeting*, A2-4, 2019.
33. M. Ameya, S. Matsukawa, and S. Kurokawa, "Uncertainty Estimation of Antenna Gain Self-Calibration Method with Moving Flat Reflector for 5G Standard Gain Horn Antenna", P*roceedings of IEEE CAMA* 2019, pp.277-280, 2019.
34. Y.She, S.Matsukawa, S.Kurokawa, "Uncertainty Analysis of Far-Field Gain Measuement of DRGH Using Single-Antenna Extrapolation Method from 1 GHz to 18 GHz," 2022 MJWRT, Malaysia, Jan, 2022 (Hybrid workshop).
35. T. Morioka, "Reflectometer calibration for net power measurement and uncertainty," in *CPEM Dig*., pp. 1-2, Denver CO, USA, Aug. 2020. (Virtual conference)
36. https://apmp-dxfg.org/dxfg-eoy-webinar-2022.html
37. https://www.dcc-conference-2023.ptb.de/home